Supporting Information (SI) to Accompany

Are Zr_6-Based MOFs Water Stable? Linker Hydrolysis vs Capillary-Force-Driven Channel Collapse

Joseph E. Mondloch,[a] Michael J. Katz,[a] Nora Planas,[c] David Semrouni,[c] Laura Gagliardi,[c] Joseph T. Hupp[a] and Omar K. Farha[a,b]

[a] *Department of Chemistry, Northwestern University, 2145 Sheridan Road, Evanston, IL 60208, United States.*

[b] *Department of Chemistry, Faculty of Science, King Abdulaziz University, Jeddah, Saudi Arabia.*

[c] *Department of Chemistry, Supercomputing Institute, and Chemical Theory Center, University of Minnesota, Minneapolis, MN 554555, United States.*

Table of Contents

S1. Materials

All compounds and solvents were used as received unless otherwise noted: 1,3,6,8-tetrakis(p-benzoic acid)pyrene was synthesized as previously described,[1] acetone (Macron, 98%), benzoic acid (Aldrich, 99.5%), 4,4'-biphenyldicarboxylic acid (bpdc) (Aldrich, 97%), benzene dicarboxylic acid (Aldrich, 98%) deuterated water (d_2-D_2O) (Cambridge, 99.9%), N,N-dimethylformamide (DMF) (Macron, 99.8%), hydrochloric acid (Aldrich, 37%), $ZrCl_4$ (Aldrich 99.5%), $ZrOCl_2 \bullet 8H_2O$ (Aldrich, 98%).

S2. Instrumentation

Powder X-ray diffraction measurements were carried out either on a Bruker MX *I*μS microsource with Cu Kα radiation and an Apex II CCD detector or on a Rigaku ATX-G equipped with a 18 kW Cu rotating anode, MLO monochromator, and a high-count-rate scintillation detector. The samples measured on the Bruker MX *I*μS were

mounted in capillaries as powders, sealed with wax and placed on a goniometer head. The data were collected on an area detector with rotation frames over 180° in ϕ and at 2θ values of 12, 24, and 36° being exposed for 10 min at each frame. Overlapping sections of data were matched, and the resulting pattern was integrated using Bruker's APEX2 phase ID program. The powder patterns were treated for amorphous background scatter. The samples measured on the ATX-G were referenced/standardized to the MOF UiO-66 as an external standard. N_2 adsorption isotherms were collected on a Tristar II 3020. Activation was performed either on a Micromertics Smart VacPrep or Micromeritics ASAP 2020 instrument. ^{1}H NMR experiments were performed on a 400 MHz Agilent DD MR-400 and referenced to the proton impurity in D_2O. Diffuse reflectance infrared Fourier transform spectra (DRIFTS) were collected on a Nicolet 7600 FTIR spectrometer equipped with an MCT detector which was cooled with liquid N_2 and the spectra were either collected under Ar atmosphere (in situ DRIFTS measurements) or in a KBr mixture under N_2 purge. KBr was utilized as a background.

S3. Synthesis of UiO-66, UiO-67, and NU-1000

UiO-66, UiO-67, and NU-1000 were synthesized as previously reported.[1-2]

S4. Activation Protocols for UiO-67 and NU-1000

The following vacuum procedures were utilized for all samples: UiO-67 was activated by first heating the sample to 90 °C (ramp rate of 2 °C min^{-1}) under dynamic vacuum until a vacuum level of 100 mmHg min^{-1} was reached. Subsequently the sample was ramped to 150 °C (ramp rate of 5 °C min^{-1}) and held until a vacuum level of < 0.005 mmHg min^{-1} was reached. NU-1000 was activated by heating to 120 °C (ramp rate of 2 °C min^{-1}) under dynamic vacuum until a level of < 0.005 mmHg min^{-1} was reached.

UiO-67 and NU-1000 were synthesized and thermally activated (*i.e.*, these are the parent "thermal activation from synthesis solvent" samples) as reported previously.[1-2] Notably, UiO-67 was activated from DMF, while NU-1000 has been activated from acetone.

For the activation experiments directly from H_2O, approximately 0.03 g of MOF was placed in 2 mL of H_2O and allowed to sit static for 24 h. The samples were activated directly from H_2O.

For the solvent-exchange experiments, approximately 0.03 g of MOF was placed in 2 mL of H_2O and allowed to sit static for 24 h. The H_2O was decanted and exchanged with 5 mL of acetone 3 times over the course of 24 h (at least one time over night). The samples were subsequently activated from acetone.

S5. PXRD Measurements

In order to compare the effect of our activation strategies we collected PXRD patterns utilizing the MOF UiO-66 as an internal standard. This allows one to more quantitatively compare the effects of activation on the crystallinity of these samples. Experimentally three separate UiO-67 containing samples were made; in each sample 0.03 g of UiO-67 (activated either from DMF, directly from H_2O, or from acetone after solvent-exchange from H_2O) and 0.024 g of UiO-66 (used as an internal standard) were weighed out into a 20-dram vial and thoroughly mixed. Three separate NU-1000 containing samples were made; in each sample 0.03 g of NU-1000 (activated either from acetone, directly from H_2O, or from acetone after solvent-exchange from H_2O) and 0.052 g of UiO-66 (used as an internal standard) were weighed out into a 20-dram vial and thoroughly mixed. In each case all of the sample was placed in a glass boat and the PXRD was collected on a Rigaku ATX-G powder X-ray diffractometer.

Qualitatively it is quite clear that the crystallinity of UiO-67 is not very well conserved upon activation directly from H_2O (Figure S1, blue line). In contrast, the crystallinity is very well conserved upon solvent-exchange to acetone (Figure S1, purple line). Nearly identical results are observed for NU-1000 (Figure S2). Quantitatively we can compare the contribution of UiO-67 and NU-1000 to the internal standard UiO-66 by fitting their contributions to the mixed PXRD patterns from the known crystal structures. The results are listed in Table S1 and clearly confirm the qualitative results shown in Figure 1 of the main text and Figure S1 and S2 of the Supporting Information.

Sample	**UiO-67 % Contribution**	**UiO-66 % Contribution**
UiO-67 As Synthesized	78.2	21.8
UiO-67 Activated from H_2O	5.7	94.3
UiO-67 Acetone Solvent-Exchange	81.6	18.4
	NU-1000 Contribution	**UiO-66 Contribution**
NU-1000 As Synthesized	85.4	14.6
NU-1000 Activated from H_2O	45.5	54.5
NU-1000 Acetone Solvent-Exchange	88.7	11.3

Table S1. A quantitative comparison of the contributions of UiO-67 and NU-1000 to an internal standard (UiO-66) after our three different activation conditions.

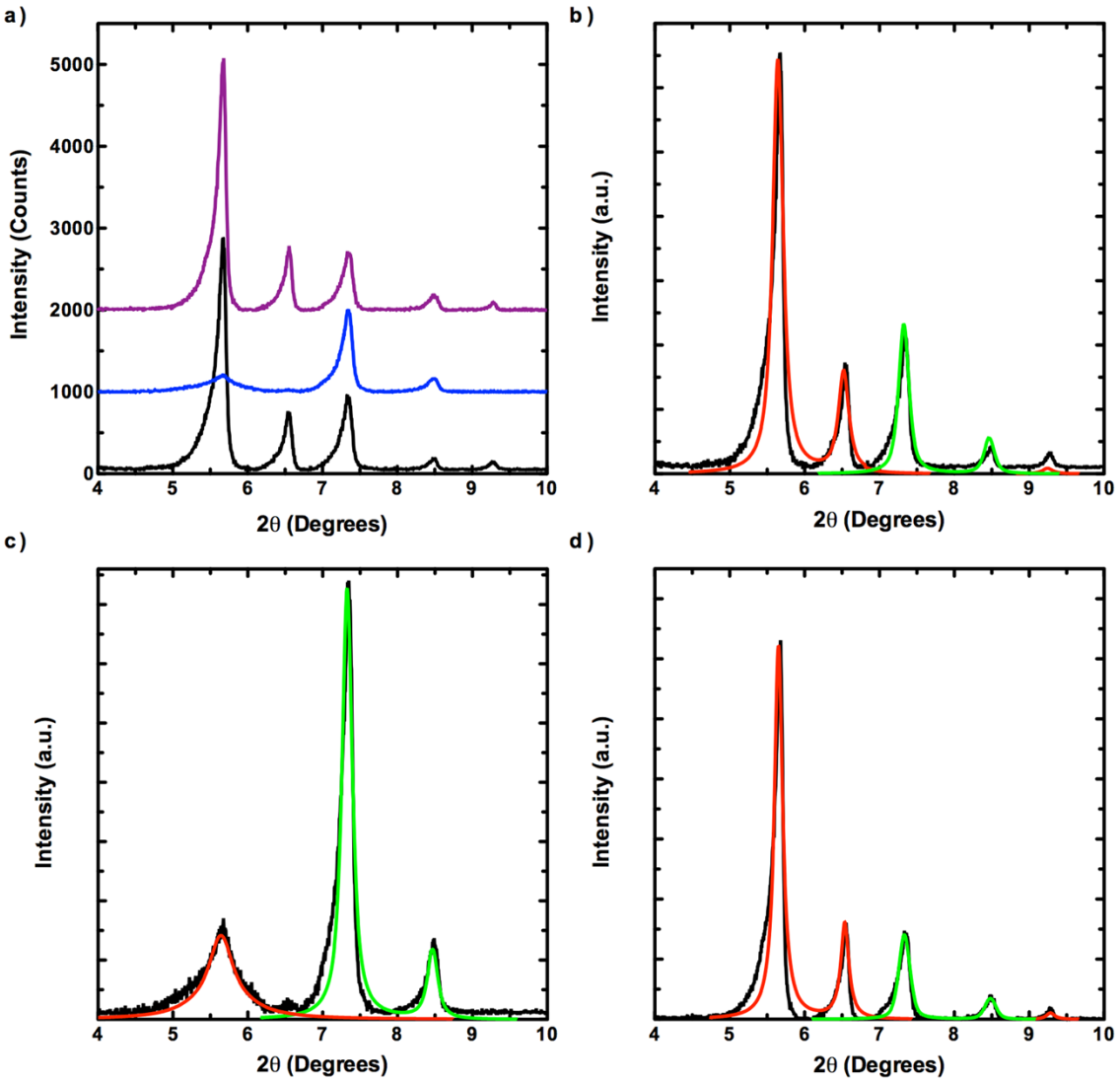

Figure S1. A comparison of the (a) absolute intensities of UiO-67 activated from DMF (black line), activated directly from H_2O (blue line), and activated from acetone after soaking in H_2O (purple line). UiO-66 has been utilized as an internal standard (7.4 and 8.5 degrees two-theta); (b) deconvolution of the contributions of UiO-67 (red line) and UiO-66 (green line) from the sample of UiO-67 activated from acetone (black line); (c) deconvolution of the contributions of UiO-67 (red line) and UiO-66 (green line) from the sample of UiO-67 activated directly from H_2O (black line); (d) deconvolution of the contributions of UiO-67 (red line) and UiO-66 (green line) from the sample of UiO-67 activated from acetone after being soaked in H_2O for 24 h (black line). The percent contributions of each component to the total PXRD pattern are summarized in Table S1.

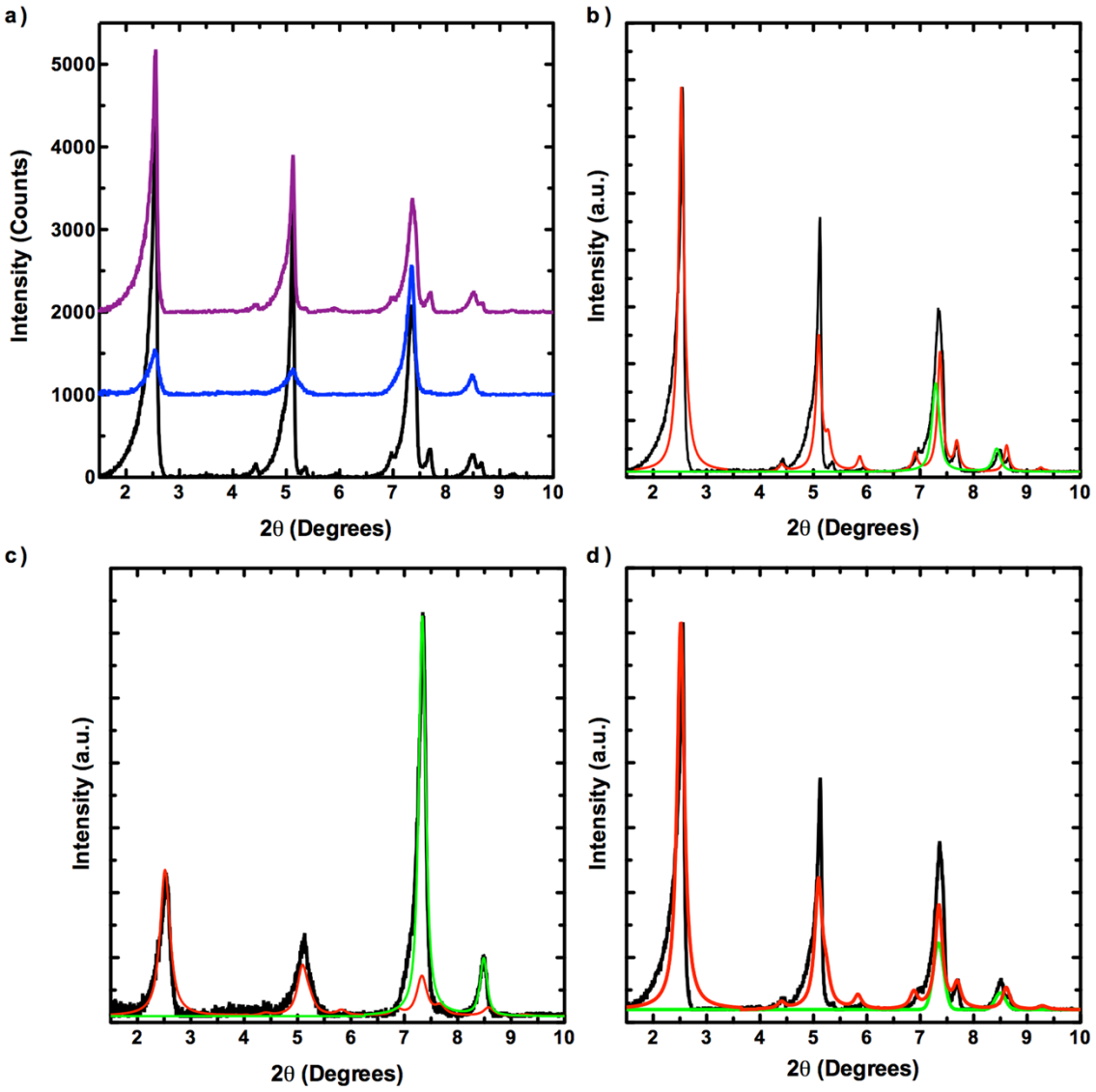

Figure S2. A comparison of the (a) absolute intensities of NU-1000 activated from acetone (black line), activated directly from H_2O (blue line), and activated from acetone after soaking in H_2O (purple line). UiO-66 has been utilized as an internal standard (7.4 and 8.5 degrees two-theta); (b) deconvolution of the contributions of NU-1000 (red line) and UiO-66 (green line) from the sample of NU-1000 activated from acetone (black line); (c) deconvolution of the contributions of NU-1000 (red line) and UiO-66 (green line) from the sample of NU-1000 activated directly from H_2O (black line); (d) deconvolution of the contributions of NU-1000 (red line) and UiO-66 (green line) from the sample of NU-1000 activated from acetone after being soaked in H_2O for 24 h (black line). The percent contributions of each component to the total PXRD pattern are summarized in Table S1.

S6. ^{1}H NMR Measurements

In order to rule out the hydrolytic degradation of UiO-67 and NU-1000 we utilized ^{1}H NMR spectroscopy. Approximately 0.015 g of UiO-67 and NU-1000 were placed in 2-dram vials and allowed to sit static in 2 mL of D_2O for 24 h. After 24 h the MOF was filtered through a 0.2 μm pipette syringe and the filtrate was collected. Small residual amounts of solvent (DMF and acetone) can be observed in the spectra. However, no resonances could be observed for biphenyl dicarboxylic acid or 1,3,6,8-tetrakis(*p*-benzoic acid)pyrene, the expected hydrolyzed linkers from UiO-67 and NU-1000 respectively.

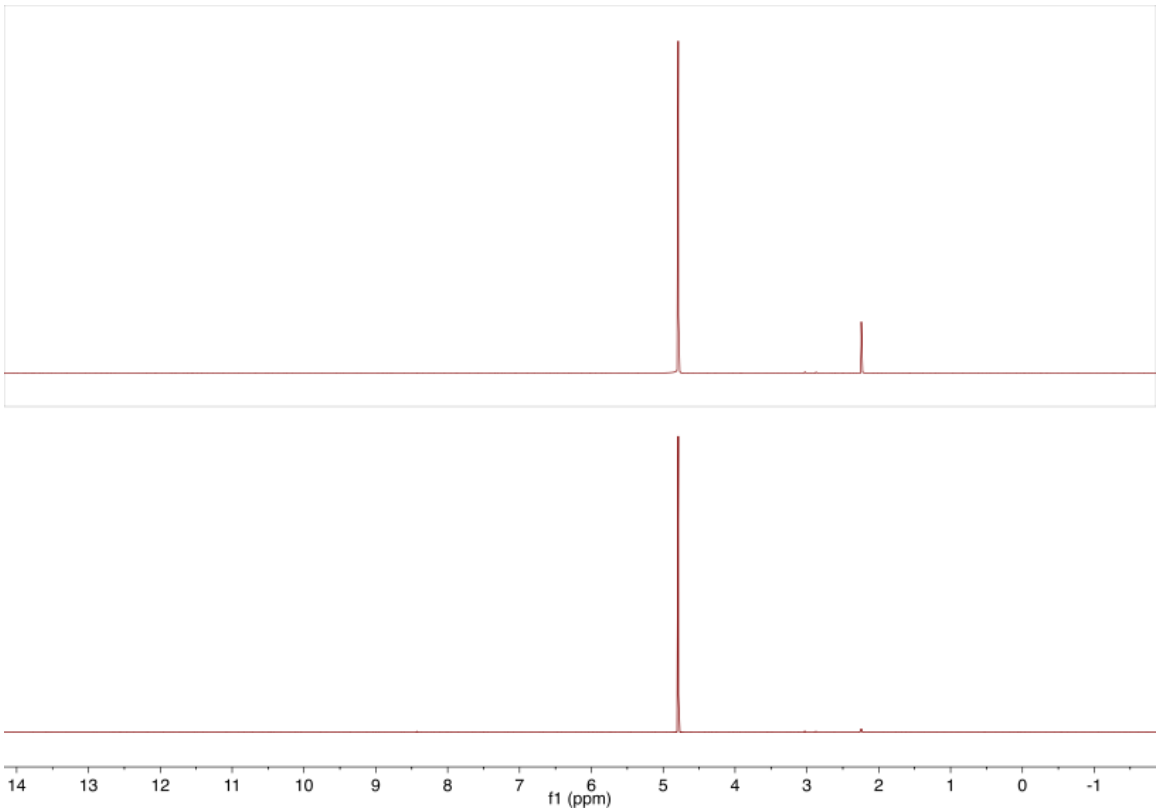

Figure S3. ^{1}H NMR spectra of the filtrate from solutions of UiO-67 (top) and NU-1000 (bottom) soaked in H_2O after 24 h.

S7. DRIFTS Measurements

Additional evidence against the hydrolytic degradation mechanism is provided by Diffuse Reflectance Infrared Fourier Transform Spectroscopy (DRIFTS). DRIFTS were recorded on a Nicolet 7600 FTIR spectrometer equipped with an MCT detector. The detector was cooled with liquid N_2. The spectra were either collected under Ar atmosphere or in a KBr mixture under N_2 purge. KBr was utilized as a background. To start we measured DRIFTS spectra of as synthesized UiO-67 and NU-1000 activated from DMF and acetone, both MOFs activated directly from H_2O, both MOFs

activated post solvent-exchange from acetone, and the free acids (Figure S4). The samples activated from the synthesis solvent and post solvent-exchange are identical. In contrast, the samples activated directly from H_2O show broad stretches from approximately 2500–3500 cm^{-1} consistent with the presence of the hydrolyzed linkers caused from the capillary forces the MOF experiences while being activated directly from H_2O.

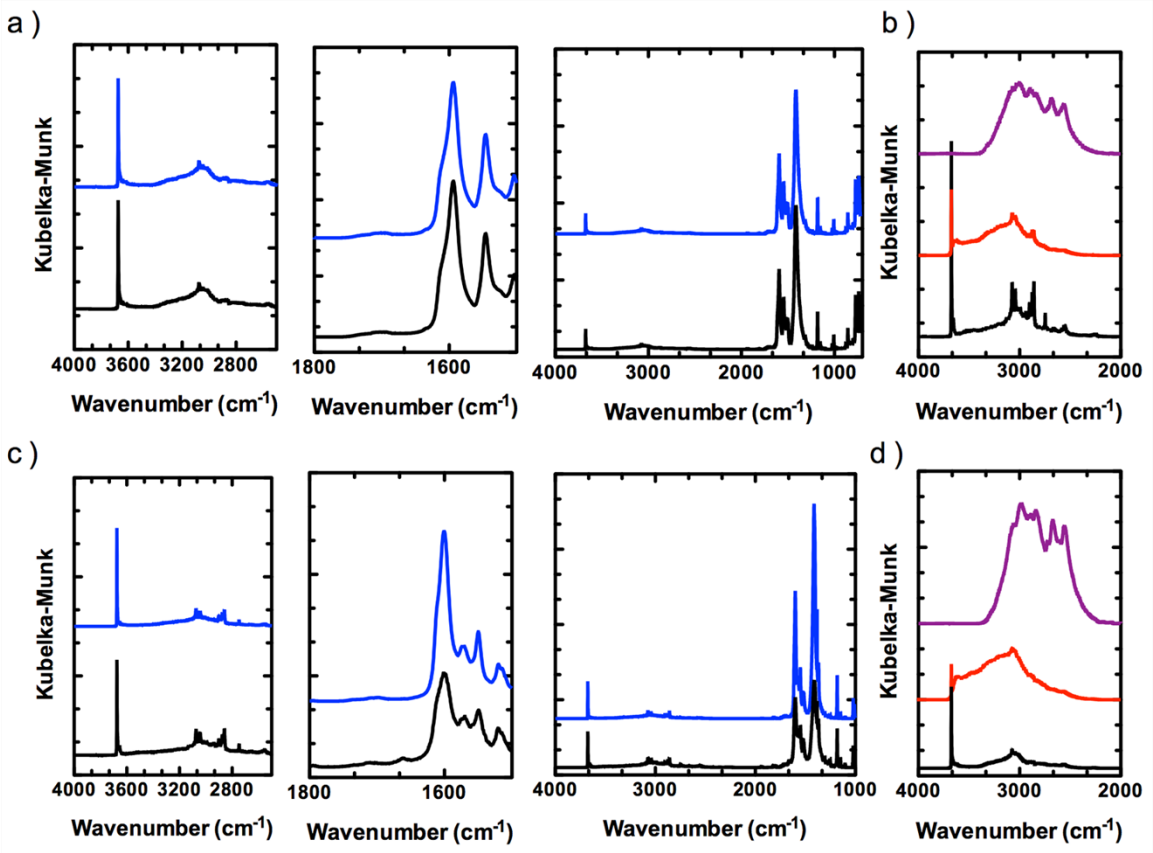

Figure S4. DRIFTS spectra of pristine UiO-67 activated from the synthesis solvent DMF (black line, a and b), UiO-67 activated directly from H_2O (red line, b), UiO-67 activated via solvent-exchange (blue line, a) and biphenyl dicarboxylic acid (purple line, b), pristine NU-1000 activated from the synthesis solvent acetone (black line, c and d), NU-1000 activated directly from H_2O (red line, d), NU-1000 activated via solvent-exchange (blue line, c) and 1,3,6,8-tetrakis(*p*-benzoic acid)pyrene (purple line, d).

We also probed the hydrolytic pathway using in situ DRIFTS measurements. UiO-67 and NU-1000 were exposed to H_2O vapor for 1h and then activated in the DRIFTS instrument at 150 °C and 120 °C respectively (Figure S5). The spectra after activation were collected after 1h at the elevated temperature. No free carboxylic acid stretching frequencies could be observed under these conditions. Maybe not surprisingly the results suggest that activation of H_2O vapor can behave differently than activation in bulk water for Zr_6-based MOFs.

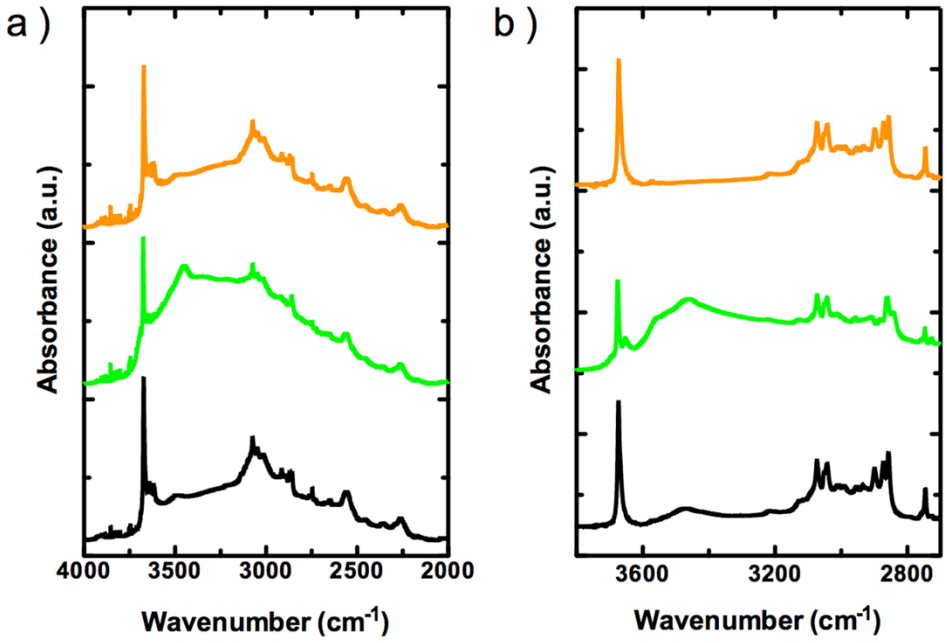

Figure S5. In situ DRIFTS measurements of UiO-67 (black line, a), UiO-67 exposed to H_2O vapor for 1h (green line, a), UiO-67 activated at 150 °C for 1h (orange line, a), NU-1000 (black line, a), NU-1000 exposed to H_2O vapor for 1h (green line, b), and NU-1000 activated at 120 °C for 1h (orange line, c).

S8. Computational Methods.

Cluster Model. From the single crystal X-ray resolved structure of UiO-67,[3] the corresponding model cluster with the general formula $[Zr_6(\mu^3\text{-}O)_4(\mu^3\text{-}OH)_4(OH)_4(OH_2)_4(PhCOO^-)_1(MeCOO^-)_{11}]$ was utilized as a starting point. For simplicity all the benzene dicarboxylate (bdc) linkers were simplified as ionic methyl acetate fragments ($MeCOO^-$) except for one linker in which has been simplified to a benzoate acetate ($PhCOO^-$) fragment, Figure S6. Notably in the main text, the methyl fragments are not shown for simplicity. The clusters were designed to maintain an overall neutral charge for the model system and to preserve a good representation of the first coordination sphere of the Zr_6 oxo-metallate nodes from the periodic structure while keeping the aromaticity of the decoordinating (bdc) ligand.

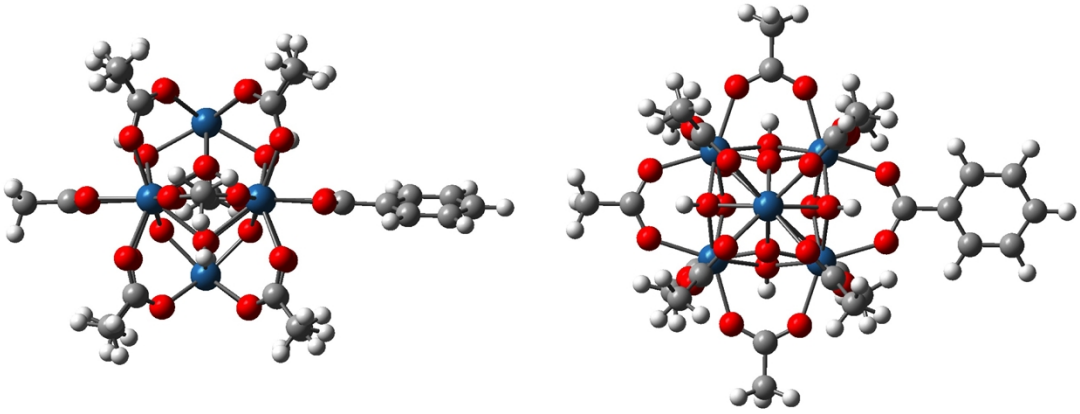

Figure S6. Ball and stick representation of two views of the cluster model for the UiO-67 node utilized to model the hydrolytic degradation. Note that the node is simplified in the main text for ease of visualization only. Color code: C, gray; H, white; O, red; Zr, blue.

Cluster Calculations. DFT cluster calculations used the M06-L[4] density functional as implemented in the *Gaussian 09* software package.[5] An ultrafine grid (99 radial nodes and 590 angular nodes) was used to perform numerical integrations. An automatic density-fitting set generated by the *Gaussian* program was used to reduce the cost for calculations done with the local density functional M06-L. The 6-31G(d,p)[6] basis set was used for H, C, N, and O while the Stuttgart [8s7p6d |6s5p3d]-GTO contracted effective core potential (SDD) basis set[7] was employed for Zr. The nature of all stationary points was verified by analytic computation of vibrational frequencies, which were also used for the computation of zero- point vibrational energies and molecular partition functions. Partition functions were used in the computation of 298 K thermal contributions to the free energy by employing the ideal-gas, rigid-rotator, harmonic oscillator approximation.[8] Single-point calculations were performed with the 6-311+G(df,p)[6] basis set for H, C, and O and the SDD basis set for Zr. The SMD continuous solvent model was employed to account for solvation with water as solvent.[9]

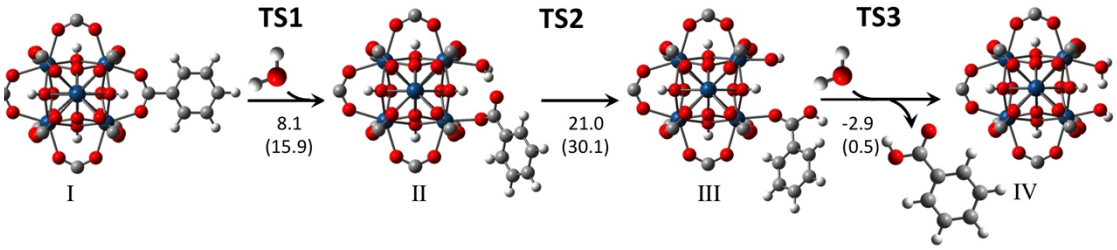

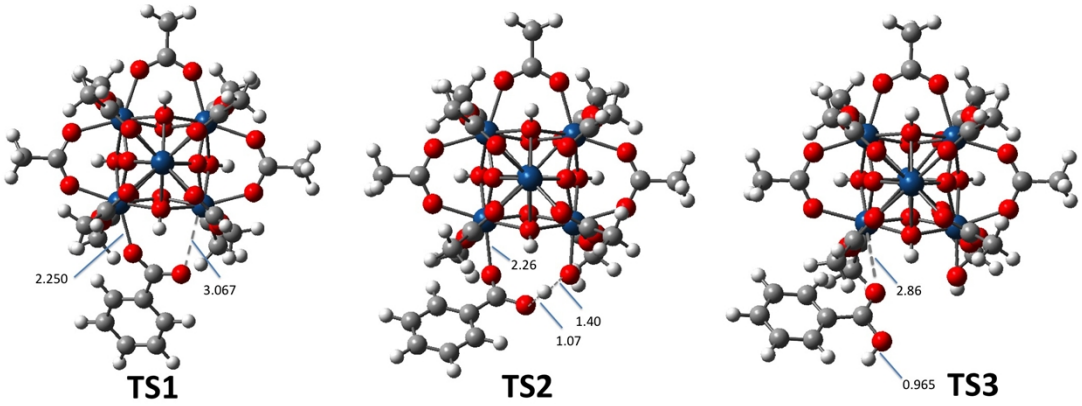

Figure S7. Top, Schematic representation of the reactions studied for the UiO-67-cluster. The node in the top of Figure S7 was simplified for clarity. Gibbs free energies in kcal/mol, activation Gibbs free energies in parenthesis. Bottom, ball and stick representation of the transition states investigated.

Estimation of the Number of H_2O Molecules in the Pores of UiO-67 and UiO-66. It is of interest to understand how H_2O molecules might behave within the pore structures of MOFs. For MOFs with a cubic unit cell like UiO-66 and UiO-67, using the solvation module of the VMD software,[10] we added water molecules to each unit cell box with periodic boundary conditions. This calculation predicts 3 and 4–5 layers of water molecules, respectively, in the pores of UiO-66 and UiO-67, respectively. We compared these results with simple geometrical considerations on UiO-66, UiO-67, NU-1000 to estimate the number of layers of H_2O molecules that can fit within each pore (i.e., double the number of H_2O layers between the center of the pore and the framework). This was done by comparing the radii of the inscribed circle within the pores of each MOF with the radius of a H_2O molecule. We find that approximately 3 and 5 layers of H_2O molecules can fit within the triangular channels of UiO-66 and UiO-67 respectively, while 5 layers and 10 layers of H_2O molecules can fit within the triangular and hexagonal channels of NU-1000 (Figure S8). In liquid water, peaks for the first and second hydration shells in the radial distribution functions at room temperature occur at about 2.8 Å and 4.5 Å, respectively.[11] Therefore, it appears that the pores of UiO-66 and UiO-67 are too small to allow for a non-truncated in-plane second hydration shell around the central water molecule. In confined water, strong distortions are observed in the H-bond network, even in the second water shell.[12] Wright et al. have shown that confined and bulk water have a similar structuration, except for a range of the order of 10 Å or less from the interface. Considering the dimensions of the hexagonal channel in NU-1000, this indicates that water in NU-1000 could have a partially liquid behavior, since it can accommodate several layers of water molecules beyond the two first shells of pore hydration.[13] Our initial study does suggest that solvent surface tension in those confined environments plays a key role in the molecular forces driving framework instability and collapse during activation. Consequently, the number of H_2O layers and their interactions with the framework should have a fundamental importance regarding the MOF stability. This

dependence is not linear. For example, NU-1000 is at least somewhat robust to activation directly from H_2O, while UiO-67 seems to exhibit complete collapse despite having less H_2O layers. However, unraveling the precise role of these H_2O–H_2O and H_2O–framework interactions on the molecular forces that give rise to framework collapse during activation are significantly beyond the scope of this manuscript. In particular, strong interactions between H_2O and the Zr_6 nodes should perturbate the hydrogen bond network and modulate our estimations and conclusions. In addition, more rigorous calculations regarding the number H_2O molecules in the Gibbs or Grand Canonical ensembles would require the development of reliable force fields for Zr_6-based MOFs. Such force fields which, to the best of our knowledge, are currently unavailable. Dynamic properties like solvent diffusion in the pores could also be computed through molecular dynamic simulations. Studies are ongoing with the aim of understanding these aspects from both a computational and experimental perspective.

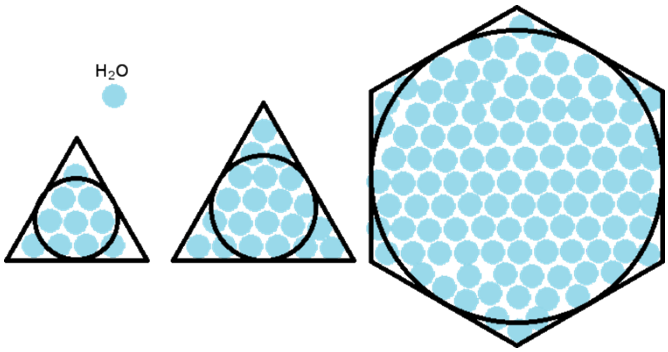

Figure S8. Scheme of inscribed circles from the left to the right, respectively of the triangular pores of UiO-66, UiO-67, and the hexagonal pore of NU-1000, compared to spherical representation of a water molecule with a radius of 1.4 Å.

S9. References

1. J. E. Mondloch, W. Bury, D. Fairen-Jimenez, S. Kwon, E. J. DeMarco, M. H. Weston, A. A. Sarjeant, S. T. Nguyen, P. C. Stair, R. Q. Snurr, O. K. Farha and J. T. Hupp, *J Am Chem Soc*, 2013, **135**, 10294.
2. M. J. Katz, Z. J. Brown, Y. J. Colón, P. W. Siu, K. A. Scheidt, R. Q. Snurr, J. T. Hupp and O. K. Farha, *Chem Commun*, 2013, **49**, 9449.
3. G. Nickerl, M. Leistner, S. Helten, V. Bon, I. Senkovska and S. Kaskel, *Inorg. Chem. Front.*, 2014, DOI: 10.1039/c3qi00093a.
4. Y. Zhao and D. G. Truhlar, *J Chem Phys*, 2006, **125**.
5. (a) M. J. Frisch, G. W. Trucks, H. B. Schlegel, G. E. Scuseria, M. A. Robb, J. R. Cheeseman, G. Scalmani, V. Barone, B. Mennucci, G. A. Petersson, H. Nakatsuji, M. Caricato, X. Li, H. P. Hratchian, A. F. Izmaylov, J. Bloino, G. Zheng, J. L. Sonnenberg, M. Hada, M. Ehara and K. F. Toyota, R.; Hasegawa, J.; Ishida, M.; Nakajima, T.; Honda, Y.; Kitao, O.; Nakai, H.; Vreven, T.; Montgomery, Jr., J. A.; Peralta, J. E.; Ogliaro, F.; Bearpark, M.; Heyd, J. J.; Brothers, E.; Kudin, K. N.;

Staroverov, V. N.; Kobayashi, R.; Normand, J.; Raghavachari, K.; Rendell, A.; Burant, J. C.; Iyengar, S. S.; Tomasi, J.; Cossi, M.; Rega, N.; Millam, J. M.; Klene, M.; Knox, J. E.; Cross, J. B.; Bakken, V.; Adamo, C.; Jaramillo, J.; Gomperts, R.; Stratmann, R. E.; Yazyev, O.; Austin, A. J.; Cammi, R.; Pomelli, C.; Ochterski, J. W.; Martin, R. L.; Morokuma, K.; Zakrzewski, V. G.; Voth, G. A.; Salvador, P.; Dannenberg, J. J.; Dapprich, S.; Daniels, A. D.; Farkas, Ö.; Foresman, J. B.; Ortiz, J. V.; Cioslowski, J.; Fox, D. J., *Gaussian 09,Revision A.02, Gaussian, Inc., Wallingford CT, 2009*, Revision A.02, (b) Y. P. Zhao, R.; Yang, K.; Truhlar, D. G., *MN-GFM 6.4.*

6. W. J. R. Hehre, L.; Schleyer, P. v. R.; Pople, J. A. , *Ab Initio Molecular Orbital Theory*, Wiley, New York, 1986.
7. D. Andrae, U. Häußermann, M. Dolg, H. Stoll and H. Preuß, *Theoret. Chim. Acta*, 1990, **77**, 123.
8. C. J. Cramer, *Essentials of Computational Chemistry: Theories and Models*, 2nd edn., John Wiley & Sons Ltd, West Sussex, 2004.
9. A. V. Marenich, C. J. Cramer and D. G. Truhlar, *J Phys Chem B*, 2009, **113**, 6378.
10. W. Humphrey, A. Dalke and K. Schulten, *"VMD - Visual Molecular Dynamics", J. Molec. Graphics*, 1996, **14**, 33.
11. (a) A. K. Soper, F. Bruni and M. A. Ricci, *Journal of Chemical Physics*, 1998, **109**, 1486, (b) A. Fouzri, R. Dorbez-Sridi and M. Oumezzine, *J Chem Phys*, 2002, **116**, 791, (c) J. Jelassi, T. Grosz, I. Bako, M. C. Bellissent-Funel, J. C. Dore, H. L. Castricum and R. Sridi-Dorbez, *J Chem Phys*, 2011, **134**, 064509.
12. A. H. Narten, *J. Chem. Phys.*, 1972, **56**, 5681.
13. D. C. Steytler, J. C. Dore and C. J. Wright, *Mol. Phys.*, 1983, **48**, 1031.